

# Honeycomb: ordered key-value store acceleration on an FPGA-based SmartNIC

Junyi Liu <i>Microsoft</i>	Aleksandar Dragojević* <i>Citadel Securities</i>	Shane Flemming* <i>AMD</i>	Antonios Katsarakis* <i>Huawei Research</i>	
Dario Korolija* <i>ETH Zurich</i>	Igor Zabolotchi* <i>Mysten Labs</i>	Ho-cheung Ng* <i>Imperial College London</i>	Anuj Kalia <i>Microsoft</i>	Miguel Castro <i>Microsoft</i>

## Abstract

In-memory ordered key-value stores are an important building block in modern distributed applications. We present Honeycomb, a hybrid software-hardware system for accelerating read-dominated workloads on ordered key-value stores that provides linearizability for all operations including scans. Honeycomb stores a B-Tree in host memory, and executes SCAN and GET on an FPGA-based SmartNIC, and PUT, UPDATE and DELETE on the CPU. This approach enables large stores and simplifies the FPGA implementation but raises the challenge of data access and synchronization across the slow PCIe bus. We describe how Honeycomb overcomes this challenge with careful data structure design, caching, request parallelism with out-of-order request execution, wait-free read operations, and batching synchronization between the CPU and the FPGA. For read-heavy YCSB workloads, Honeycomb improves the throughput of a state-of-the-art ordered key-value store by at least  $1.8\times$ . For scan-heavy workloads inspired by cloud storage, Honeycomb improves throughput by more than  $2\times$ . The cost-performance, which is more important for large-scale deployments, is improved by at least  $1.5\times$  on these workloads.

## 1 Introduction

In-memory key-value stores are an important building block in modern distributed applications [7, 9, 14, 42, 50]. They store data in servers that provide a simple interface ( $\text{PUT}(K, V)$ ,  $\text{V}=\text{GET}(K)$ ,  $\text{UPDATE}(K, V)$  and  $\text{DELETE}(K)$ ) to clients across the network. Ordered key-value stores expand the set of supported applications by providing an efficient SCAN operation to retrieve the key-value pairs whose keys are within a specified range. For example, distributed file systems can use SCAN to map ranges of logical file offsets to the nodes storing the data [9]. It is also used to query graph stores [7, 50] and the popular Redis [14] offers sorted sets. We describe Honeycomb, a system that provides hardware acceleration for an in-memory ordered key-value store.

\*This work was done when affiliated with Microsoft

†This work has been submitted to the IEEE for possible publication. Copyright may be transferred without notice, after which this version may no longer be accessible.

There is a large body of research on improving the performance of ordered key-value stores, e.g., [12, 18, 29, 38, 41, 52, 56]. Recent research has shown how to leverage modern networks to achieve high throughput and low latency with an RPC-based system [29]. Other research has explored using one-sided RDMA reads to bypass the server CPU for GET and SCAN operations [12, 18, 41, 52, 56]. Since RDMA NICs only provide simple one-sided reads of contiguous memory regions, these systems require at least two RDMA reads per operation when supporting variable-sized keys or values, and they require client-side caching to avoid additional RDMA reads when traversing the tree data structures stored by the servers.

Honeycomb accelerates an ordered key-value store using an FPGA-based SmartNIC [10, 45] attached to a host CPU. These SmartNICs are widely deployed in data centers [10, 20–22, 45]. They enable effective CPU offload by avoiding the functionality limitations of RDMA and the performance problems of SmartNICs based on general-purpose, low-power cores [8]. Previous work used a similar SmartNIC to accelerate an unordered key-value store [35]. Honeycomb solves a harder problem because ordered key-value stores use more complex data structures whose operations perform  $O(\log(n))$  memory accesses instead of the  $O(1)$  accesses performed by hash table operations in unordered key-value stores.

Honeycomb implements the ordered key-value store using a B-Tree [13] that supports variable-sized keys and values that are stored inline in B-Tree nodes to improve the performance of scans. It uses multiversion-concurrency control (MVCC [5]) to provide linearizability [25] for scans. This is important to provide strong consistency, e.g., in the distributed file system example above, clients may fail to read previously written data when scans are not linearizable.

Honeycomb stores the B-Tree in host memory. It accelerates GET and SCAN operations by executing them on the FPGA, but PUT, UPDATE and DELETE operations are executed by the host CPU. Since most workloads are read-dominated [4, 15, 17, 34, 50], there is less benefit in accelerating write operations and the cost of accelerating them in hardware is high because they may require complex splitting and merging of B-Tree nodes. This hybrid approach enables much larger stores than would be possible using the limited DRAM attached to the FPGA and it reduces the complexity of

the FPGA implementation. However, it brings the challenge of data access and synchronization across the slow PCIe bus. We overcome this challenge with careful co-design of the software running on the CPU and the FPGA hardware image.

Honeycomb uses several techniques to reduce data accesses over PCIe. It caches B-Tree nodes on both FPGA SRAM and on-board DRAM. It also uses large B-Tree nodes with *shortcuts*, a list of sorted keys and offsets into the node that divide it into segments of similar size. This allows requests to fetch only the relevant segments of each node they access, which reduces the number of bytes accessed to search for a key and the total amount of memory required to cache interior nodes compared to simply using smaller nodes.

To use available off-chip FPGA bandwidth efficiently, Honeycomb exploits request-level parallelism and avoids head of line blocking with out-of-order request execution. To use all available off-chip bandwidth, Honeycomb also implements a dynamic load balancer that directs some requests that hit on the cache to host memory if there is no bandwidth available to on-board DRAM and there is unused bandwidth over PCIe.

Honeycomb reduces the cost of synchronization across PCIe by making GET and SCAN operations wait free [24]. It also divides each leaf B-Tree node into a *sorted block* with sorted key-value pairs and a small *log block* that logs recent PUT and DELETE operations. The log block is merged into the sorted block when its size exceeds a threshold. This ensures reads traverse mostly sorted items while avoiding sorting the node and synchronizing the CPU and the FPGA on each write.

A comparison with a state-of-the-art ordered key-value store, which uses eRPC [29] and Masstree [38], shows that Honeycomb improves both peak performance and cost-performance, which is more important in large-scale data centers [28], significantly for scan-dominated workloads. For example, in uniform workloads with inserts and short scans, Honeycomb improves the throughput by  $1.2\times$  for workloads with 50% reads and by more than  $2.3\times$  for workloads with at least 80% reads. Most importantly, Honeycomb improves throughput per watt of Thermal Design Power (TDP), which is a proxy for total cost of ownership [28], by more than  $1.9\times$  for workloads with at least 80% reads. We expect these gains to increase with future hardware because newer FPGAs have more on-chip memory to cache B-Tree nodes and they are connected to the host using PCIe Gen5 that has four times higher bandwidth than the PCIe Gen3 used in our system.

We describe the architecture of Honeycomb in Section 2, the algorithms and data structures used to implement the B-Tree in Section 3, and how these are implemented in hardware in Sections 4 and 5. Section 6 presents the evaluation.

## 2 Honeycomb architecture

Figure 1 shows the architecture of Honeycomb: an FPGA-based SmartNIC that connects a host server to the datacenter network. The Honeycomb accelerator is built on the Catapult

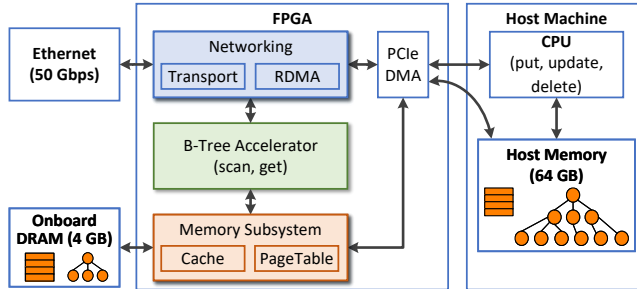


Figure 1: Hardware system architecture.

FPGA infrastructure [10, 45], which provides a shell with IO support. The core FPGA image has three subsystems: the B-Tree accelerator, networking, and memory.

The B-Tree is stored in host DRAM because it scales to much larger capacities than on-board DRAM in FPGAs. The B-Tree accelerator implements GET and SCAN operations and PUT and DELETE operations are executed by the CPU.

The networking subsystem implements LTL [10], a UDP-based transport protocol similar to RoCE v2 [55] on top of 50 Gbps Ethernet, and an RDMA engine to enable efficient host-to-FPGA communication. The RDMA engine supports custom commands for GET and SCAN in addition to general commands like READ, WRITE, SEND, and RECEIVE. These enable kernel bypass at the clients and at the servers for PUT, UPDATE and DELETE. They also enable the B-Tree accelerator to completely bypass the CPU for GET and SCAN requests by receiving these commands directly from the network subsystem, processing them, and sending back replies.

The memory subsystem interfaces with host memory over PCIe and with on-board DRAM. It maintains a cache and a page table. The cache stores interior B-Tree nodes in on-board DRAM and the root of the B-Tree in on-chip SRAM. The page table simplifies atomic updates to the B-Tree (Section 3.4) by adding indirection [34]. It is stored in on-board DRAM and maps logical identifiers (LIDs) for B-Tree nodes to their physical addresses in host memory.

The FPGA is connected over two PCIe Gen 3  $\times 8$  to the host. We measured a peak throughput of 13 GB/s and a latency of more than  $1 \mu\text{s}$  (depending on load). For comparison, the bandwidth between host CPU and DRAM is up to 64 GB/s with an order of magnitude lower latency, and CPU cores have large caches that improve performance further. Therefore, Honeycomb must address the challenge of data access and synchronization across the PCIe bus to achieve performance and cost-performance gains relative to CPU-only systems. The next sections describe how we overcame this challenge with careful hardware-software co-design.

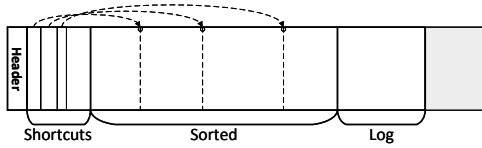


Figure 2: Honeycomb node layout.

### 3 B-Tree

Honeycomb implements a B+ tree [13], i.e., key-value pairs (also called items) are stored only in leaf nodes while interior nodes store keys and pointers to child nodes. Honeycomb guarantees linearizability [25] for all operations including scans.

#### 3.1 Node layout

B-Tree nodes are fixed-size, which is configured to 8 KB in this paper. They are allocated in pinned host memory to allow the FPGA to use physical memory addresses directly. B-Tree nodes do not store addresses of child or sibling nodes directly. Instead, they store 6-byte logical identifiers (LIDs) [34]. The mapping from a LID to the virtual and physical addresses of a node is maintained in a page table.

The node layout is shown in Figure 2. The node header is stored in the first 48 bytes. It contains fields specifying the node type (interior or leaf), the number of bytes used, a lock word, and a version number to synchronize accesses to the node. The header of an interior node stores the LID of the leftmost child. The header of a leaf node stores the LIDs of the siblings to improve scan performance. Leaf nodes store keys and values in variable-size blobs. Each blob has a 2-byte header that specifies its size. Keys and values are stored inline in B-Tree nodes to improve performance. In the current configuration, the maximum key length is 460 bytes and values larger than 469 bytes are stored outside the node.

Leaf nodes are split in two blocks: sorted and log. The pointer to the boundary between them is stored in the node’s header. The sorted block stores items in ascending lexicographic order of keys and the log block stores a log of recent changes. When the log block grows larger than a threshold (currently set to 512 bytes), it gets merged with the sorted block. Therefore, read operations benefit from accessing mostly sorted data and write operations avoid the overhead of sorting the node on every change. It also reduces synchronization across PCIe because it requires one update to the FPGA page table per-merge instead of one on every write operation.

Since interior nodes change infrequently, the cost of storing a log block and accessing it on reads outweighs the benefits. Therefore, interior nodes do not have log blocks.

Entries in the log block are either newly inserted or updated items or delete markers. Each entry stores a 2-byte pointer to an item in the sorted block. For a newly inserted item, it points

to the first item with key greater than the item’s key. For other entries, it points to the deleted or updated item. In addition, each entry records the 1-byte index in the sorted order of log items at the time of insertion. These fields are used to sort all node items, when searching the leaf, without comparing keys and with  $O(1)$  cost per log block item (Section 4.3).

To optimize the search for a key in a node, we split the sorted block into segments of roughly equal size. We store the keys at the boundaries of segments and the pointers to the boundaries in the shortcut block, which is stored immediately after the node header. We currently reserve 48 bytes for the header and 464 bytes for the shortcut block. The shortcut keys are selected during the merge of the sorted and log blocks. They are stored only in the shortcut block, i.e., the start of the segment for boundary key  $K$  contains the value associated with  $K$  rather than another copy of  $K$  followed by the value.

The search for a key starts by traversing the shortcut block to identify the segment that contains the key. The search examines only that segment and the log block, which reduces the amount of data read both from host memory and the cache. Since Honeycomb’s bottleneck is FPGA off-chip bandwidth, this optimization significantly improves performance. For small keys with the current configuration, a search reads at most 1.5 KB of data from an 8 KB node, which is a  $5\times$  performance improvement relative to reading the whole node.

Analysis shows that using large nodes with shortcuts reduces the number of bytes accessed to search for a key and the total amount of memory required to cache interior nodes compared to simply using smaller nodes. For the example of a five-level tree with 8 KB nodes, 16-byte keys and values at 55% occupancy, searching the tree with this optimization accesses fewer than 75% of the bytes accessed searching a simple tree with 512-byte nodes with a similar number of items. It also requires approximately four times less space to cache all the interior nodes. The intuition is that the FPGA can use the information in the header to fetch a sorted block segment or a log block with a single DMA that reads only the bytes in use, whereas it would need to read the whole node or issue more dependent DMAs for the simple tree. Also using smaller nodes increases overhead because it requires more storage for pointers to children in interior nodes. Using log blocks reduces the impact of sorting the large node on writes.

#### 3.2 Synchronization

GET and SCAN operations executed by the accelerator are wait-free [24] – they never block or retry due to PUT or DELETE operations executed by the CPU. This reduces the overhead of synchronization over PCIe and provides predictable latency.

We use multi-version concurrency control (MVCC) [5] to ensure that read operations can always access a consistent snapshot of data. Honeycomb maintains two shared 64-bit version numbers: the *global write version* and the *global read version*. A write operation performs an atomic fetch and add

on the global write version to obtain its write version, which is used to version any items it creates. Writers *release changes* to readers in version order: a writer sets the global read version to its write version when it becomes the writer with the smallest write version, and updates the copy of the global read version maintained by the accelerator over PCIe. We delay responses to write requests until this update completes. Writers synchronize with each other using node locks, which are ignored by readers. Read operations read the global read version maintained by the accelerator to get their read version. They ignore items with versions greater than this value.

All items in the sorted block have the same version that is stored in the node header and is called the *node version*. The node version is the write version of the write operation that created the version of the node. Nodes also store a pointer to the state of the node as of the previous version. A reader that observes a node version greater than its read version follows the chain of old version pointers until it reaches a node with a version less than or equal to its read version. The version of an item in the log block is stored in the item header. To reduce the size of these headers, we store a 5-byte version delta from the node version instead the entire 8-byte version. If a write would cause the delta version to wrap around, it merges the sorted and log blocks. Readers ignore all items in the log block with versions greater than their read version.

To ensure operations observe a consistent snapshot, Honeycomb does not reclaim old versions of nodes while at least one in-flight operation can access a snapshot to which the old version belongs. To garbage collect old versions that are not accessible anymore, Honeycomb uses an epoch-based memory manager [39]. Each CPU thread executes operations one at a time, assigns a sequence number to each in-flight operation, and exposes its current operation sequence number to the memory manager. Similarly, the B-Tree accelerator assigns a sequence number to each operation and exposes the sequence numbers of the newest and the oldest in-flight operation to the memory manager over PCIe. When a CPU thread makes a change that removes old versions of nodes from the tree, it puts the old versions into a garbage collection list tagged with a vector timestamp. This vector timestamp has entries for the current operation sequence numbers of all CPU threads and the newest operation sequence number on the accelerator.

Periodically, a thread scans the garbage collection list and reclaims all node versions that are not reachable by CPU threads or the accelerator, i.e., node versions with a vector timestamp where the entry for each CPU thread is smaller than the current operation sequence number for the thread, and the entry for the accelerator is smaller than the current oldest in-flight operation on the accelerator. If a writer fails to allocate memory for a new node and the garbage collection list is not empty, the operation is aborted and retried.

The page table is stored both in host DRAM and in FPGA on-board DRAM. When a new node mapping is created or when a node's mapping is changed, the CPU updates the table

in host memory and issues a PCIe command to the FPGA to update the copy of the table in FPGA on-board memory.

Honeycomb can be configured with MVCC off by using zero as the version number for all nodes and log items, and by not setting old version pointers. This improves write performance a little by avoiding updates to the global read version on the FPGA. The atomic tree updates using the page table still ensure linearizability for GET, PUT, and DELETE, but not for SCAN because sibling pointers are not updated atomically.

### 3.3 Scan and get

Honeycomb implements  $\text{SCAN}(K_l, K_u)$  that finds the largest key  $K_s$  less than or equal to  $K_l$ , and returns a sorted list with all key value pairs with keys greater than or equal to  $K_s$  and less than or equal to  $K_u$ . We implement this version of SCAN to support mapping from a range of logical file offsets to the nodes storing the data in distributed file systems [9]. In this application, the key-value pairs represent variable-sized chunks of file data where the key is the logical offset of the first byte in the chunk and the value points to the servers storing the data. Since the start of a logical file offset range in a client request can be in the middle of a chunk, the SCAN semantics we implement are necessary for correctness.

$\text{SCAN}(K_l, K_u)$  traverses the tree from the root to a leaf. It fetches the node header and shortcut block of each node it visits (currently stored in the first 512 bytes). It follows old version pointers if needed to find a node with version less than or equal to the operation's read version. Then it searches for the largest shortcut key less than or equal to  $K_l$ , and fetches the associated sorted block segment. When SCAN visits an interior node, it searches the segment for the item with the largest key less than or equal to  $K_l$  (which could be the shortcut key), and obtains the LID of the next node to visit from the item.

When SCAN reaches the leaf, it fetches the log block in parallel with searching the shortcuts. Then it searches both the sorted and log blocks for the largest key  $K_s$  less than or equal to  $K_l$ . It scans forward from  $K_s$  until it reaches a key greater than  $K_u$  or the end of the tree. It ignores any items with versions greater than the read version. If it finds one or more items with the same key, it returns the value associated with the item with the latest version unless that item is a delete. Otherwise, it ignores the item. SCAN uses sibling pointers to move to the next leaf if needed.

The accelerator optimizes scan performance by determining a sorted order for the items in the log block of a leaf, and uses the back pointers from log block items to sorted block items to determine a sorted order across all the items in the leaf (see Section 4.3). This enables efficient scanning by overlapping data access with key comparisons, generating results that are already sorted, and avoiding key comparisons with all items in the log block.

Honeycomb implements  $\text{GET}(K)$  as  $\text{SCAN}(K, K)$  and post-

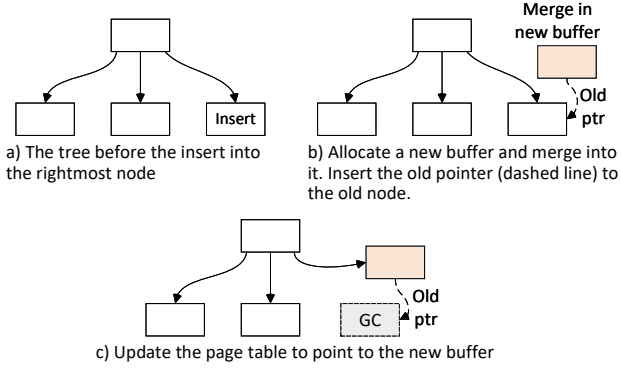


Figure 3: Merging the sorted and log blocks.

processes the result to return the value associated with  $K$ , or return not found if  $K$  is not in the result.

### 3.4 Insert

A  $PUT(K, V)$  operation inserts a new item if there is no item with key  $K$  in the tree. It traverses the tree as described for  $SCAN(K, K)$  without acquiring any locks, but it reads the latest version of each node to implement linearizability. The operation locks the leaf node before modifying it to ensure the state matches the one observed during the traversal.

The node header has a 32-bit lock word with a lock bit and a 31-bit sequence number, which is incremented on writes to the node.  $PUT$  tries to acquire the leaf's lock using an atomic compare-and-swap instruction that checks if the sequence number matches the one observed during the traversal. If the compare-and-swap fails, the  $PUT$  operation restarts.

**Fast-path insert:** In the common case, the operation simply adds a new item to the log block: it copies the item to the log block; acquires the write version with a fetch-and-add on the global write version; sets the version of the item in the log block; updates the node size; increments the node sequence number; and unlocks the node. The node size and the lock word are packed into a 64-bit word. So that the last three steps can be performed with a single instruction. Concurrent operations either observe the node without the item or with the item correctly written, and readers ignore the item until the change is released (Section 3.2).

**Sorted and log block merge:** If the size of the log block exceeds a threshold (currently 512 bytes), the operation merges the sorted and log blocks as shown in Figure 3. It allocates a new memory buffer for the node and sorts all the items into a single sorted block in the new buffer. While sorting, it selects the shortcut keys. For each item, it decides whether to put the key in the shortcut block based on the number of bytes copied so far, the remaining bytes to copy, and the average size of keys and values. It attempts to maximize the number of shortcut keys while ensuring that segments have similar sizes, a minimum size (currently 256 bytes), and that

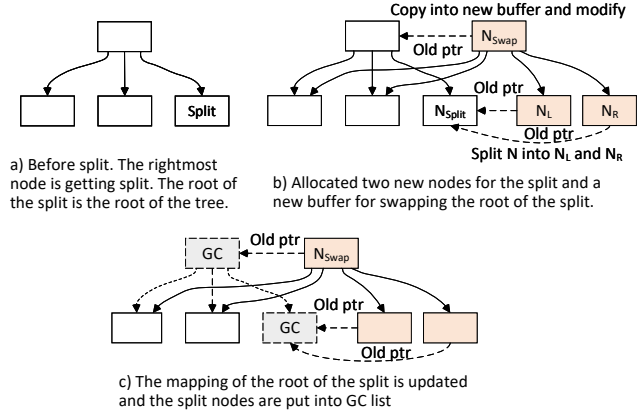


Figure 4: Splitting a node during insert.

shortcut keys fit in the shortcut block.

The operation sets the node version to the write version, and the old version pointer to the address of the old buffer (Figure 3b). Then it updates the LID mapping with the address of the new buffer in the page tables of both CPU and FPGA (Figure 3c). The parent node does not need to be changed because the LID of the child remains the same. The operation also puts the old buffer in the garbage collection list and releases the changes to make them visible to readers. This ensures concurrent operations observe the change atomically.

**Node splitting:** If there is not enough space in the leaf for the merged block, the operation splits the leaf in two. This requires inserting a new item in the parent node as shown in Figure 4. If the parent is full, the operation also splits the parent. Splitting can propagate to the root. The last interior node that is updated but not split is called *the root of the split*.

The operation acquires locks on all interior nodes to split and on the root of the split. If locking fails due to a sequence number mismatch, it releases all acquired locks and restarts. The operation also allocates two new nodes (new LID and memory buffer) for each node that it splits and a memory buffer (same LID) for the root of the split ( $N_L$ ,  $N_R$ , and  $N_{swap}$  in Figure 4b). Then it processes nodes from the leaf up splitting the items in each node evenly into the two newly allocated nodes. When it gets to the root of the split, the operation copies the items into the new buffer and adds the LIDs of the new child nodes and the key at the boundary between them.

To swap in the new subtree atomically, the operation updates the LID mapping for the root of the split in both CPU and FPGA page tables to point to the new buffer (Figure 4c). It also locks the sibling leaves and updates their sibling pointers to point to the new leaves. This is sufficient to ensure linearizability for all operations but scans, because the updates to the sibling leaves and the subtree swap are not atomic.

Linearizable scans are important for applications like the distributed file system [9]. Without them, a client  $C$  could write data  $D$  to a file at a logical offset range  $R$ , and a later

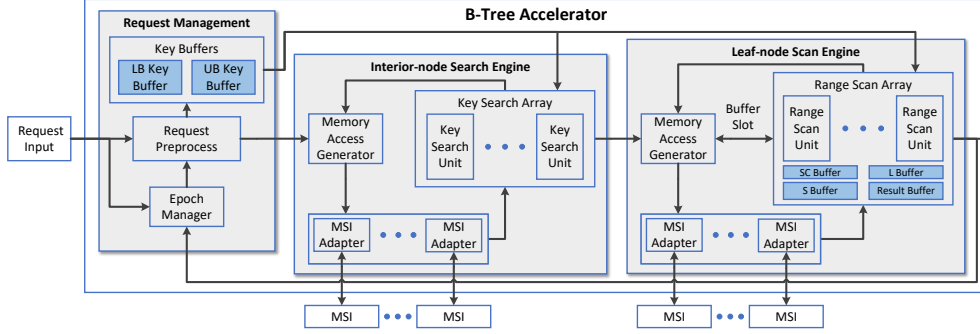


Figure 5: B-Tree accelerator architecture.

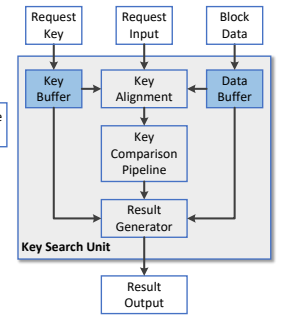


Figure 6: Key search unit

read from a range containing  $R$  could fail to return  $D$ . This can happen if the B-Tree node with the mapping for the servers that store  $D$  is split and the sibling pointers are not updated before the scan to find the servers storing the data being read.

To provide linearizable scans, the operation sets the versions in all newly allocated buffers to its write version, and sets the old version pointer in the new root of the split to the address of the old buffer (Figure 4b). This ensures that operations with older read versions traverse the old subtree. It also sets the old version pointers of the new leaves to the address of the old leaf. This ensures that scans with older read versions, which may reach the new leaves using sibling pointers, traverse the old leaf. The operation also puts the LIDs and memory buffers of all nodes that got split, and the old memory buffer of the root of the split in the garbage collection list. The operation then unlocks all nodes and releases the changes to readers (Section 3.2). This ensures readers observe all changes made during the split, or none of them.

If the tree root must be split, the operation grows the tree by allocating a LID and a memory buffer for the new root, and updating the root and tree height in the accelerator.

### 3.5 Delete and update

The implementations of UPDATE and DELETE are similar to INSERT. UPDATE appends the updated key-value pair to the log block, which points to the previous version of the item in the sorted or log block. For DELETE, a delete marker is appended in the same way to indicate that readers should ignore the deleted item. The space for stale and deleted items is reclaimed when merging the sorted and log blocks. Nodes whose occupancy drops below a threshold are merged and nodes that become empty are deleted. We use similar techniques to ensure atomicity as for splits but omit the details.

## 4 B-Tree accelerator implementation

The B-Tree accelerator has three components (Figure 5): request management, interior-node search engine, and leaf-node scan engine. Request management parses requests and assigns

them sequence numbers and read versions. The interior-node search engine is responsible for traversing the tree from the root to a leaf. The leaf-node scan engine traverses the leaf or, for SCAN operations, leaves using sibling pointers.

### 4.1 Request management

The time to complete requests is variable, e.g., due to different size keys or cache misses. Therefore, the B-Tree accelerator exploits request-level parallelism and avoids head of line blocking by supporting out-of-order request execution. This maximizes the utilization of compute resources, and on-board DRAM and PCIe bandwidth.

The request pre-process module extracts the lower (LB) and upper bound (UB) keys from the request and stores them in centralized key buffers. These buffers support multiple read ports to enable the interior-node search engine and the leaf-node scan engine to read multiple keys in parallel. When a request completes, its key buffers are freed.

The request pre-process module also initializes *request metadata* that includes: identifiers of the buffers holding the keys, the LID of the node being traversed, the node’s level, the block type being traversed (shortcut, sorted, or log), and the start offset of the block/segment within the node. The request metadata flows over a wide data path through the accelerator.

Request management is also responsible for storing the accelerator’s copy of the 64-bit global read version, which is updated by the CPU over PCIe (Section 3.2). It reads the global read version to assign a read version to each incoming request. Requests are also assigned a 64-bit sequence number by incrementing a counter  $S_{new}$  maintained by the epoch manager. These are part of the request metadata.

The epoch manager also monitors request completion to keep track of  $S_{old}$ , the sequence number of the oldest inflight request. It exposes  $S_{old}$  and  $S_{new}$  over PCIe to the memory manager running on the CPU to enable reclaiming memory when it is no longer accessible by inflight requests (Section 3.2). Accesses to  $S_{old}$  and  $S_{new}$  over PCIe are infrequent.

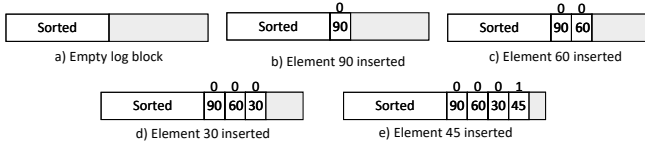


Figure 7: Example of order hints in the log block.

## 4.2 Interior-node search engine

The interior-node search engine is responsible for traversing interior nodes from the root as described in Section 3.3. It uses a ring architecture to search node blocks iteratively while overlapping memory reads with compute (Figure 5). The architecture exploits request-level parallelism by using multiple memory subsystem interface (MSI) adapters and key search units (KSU). Additionally, each MSI adapter supports out-of-order data transfer to fully utilize off-chip bandwidth.

For each interior node visited by a GET or SCAN request, the memory access generator first generates a memory access request to one of the MSI adapters to fetch the node’s header and shortcut block. The adapter issues the request to the memory subsystem, waits for the response, and sends the response to one of the KSU. The KSU first checks if the version in the node header is greater than the request’s read version. If so, it sends the updated request metadata back to the memory access generator to visit the old version of the node. If not, the KSU searches the shortcuts for the sorted block segment to fetch. Then sends the updated metadata back to the memory access generator that generates a memory access request to one of the MSI adapters to fetch the sorted block segment. When the adapter gets the segment, it is sent to one of the KSU. The KSU searches the segment for the LID of the next node to visit. If the next node is a leaf, the request is passed on to the leaf-node scan engine. Otherwise, the request is passed to the memory access generator to continue with the child.

The architecture of a KSU is shown in Figure 6. It uses the request input metadata to fetch the request’s lower bound key. Then it processes the block data (header and shortcut, or sorted block segment) to find the largest key that is smaller than or equal to the request key. Since keys are variable size, KSU have to process keys sequentially. They process keys in a streaming fashion overlapping data transfer with key comparisons. The key comparison pipeline implements comparison logic equivalent to the C++ `memcmp()` function. It compares key fragments stored in registers with configurable width (currently 16 bytes). Key alignment uses barrel shifters to stream keys into the comparison pipeline. The result generator outputs updated request metadata.

## 4.3 Leaf-node scan engine

The leaf-node scan engine is responsible for traversing leaf nodes as described in Section 3.3. As shown in Figure 5, it also uses a ring architecture to scan leaf node blocks iteratively,

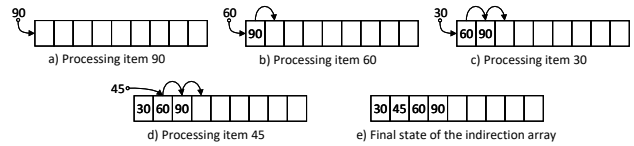


Figure 8: Sorting the log indirection array with order hints.

and exploits request-level parallelism by using multiple MSI adapters and range scan units (RSU).

Unlike the key search array, the range scan array includes several buffers: *result buffer*, *SC buffer*, *S buffer*, and *L buffer*. The result buffer is used to accumulate partial results because the leaf-node scan engine produces a sorted list of key-value pairs spread across different blocks in one or more leaves. The SC buffer, S buffer, and L buffer are used to buffer data from shortcut, sorted, and log blocks in a leaf, respectively. This enables iteration over keys in the three blocks in a sorted order to generate sorted results. The range scan array also includes different RSU variants to scan each type of block and finite state machines (FSM) that coordinate scans across the three RSU variants. The buffers are separate from RSUs to enable overlapping of compute with data buffering. The buffers are divided into request slots that also include the FSM state. The memory access generator maintains a list of available slots. It assigns slots to requests or pushes back if no slot available.

The architecture of the RSU is similar to the KSU (Figure 6) but it has two parallel key comparison pipelines to compare keys with both the lower and upper bound keys in the SCAN operation. Additionally, the RSU variant responsible for log block processing must first sort the log block to enable iterating over the key-value pairs in order.

We leverage hardware-software co-design to optimize log block sorting. Sorting does not compare keys and costs only  $O(1)$  cycles per item. It uses 1-byte order hints stored in log block items by inserts. Figure 7 illustrates an example sequence of insertions into the log block. For clarity, the number in the item represents its key. The number above the item represents its order hint. The log block is initially empty. Item 90 is inserted first and is assigned order hint 0. Next, item 60 is inserted. Since it is the smallest item in the log block, it is assigned order hint 0. The order hints in existing items are not changed. Then, item 30 is inserted with order hint 0 since it is the smallest in the log block again. The final item is 45 and its order hint is 1.

Sorting creates an indirection array with offsets of items in the log block in ascending key order. Figure 8 illustrates sorting of the log block in Figure 7. It shows keys instead of item offsets for clarity. Items are processed in the order in which they are stored. When the item with order hint  $i$  is processed, its offset in the log block is inserted into position  $i$  in the indirection array and all the elements at positions  $j \geq i$  are shifted to the right. Since the indirection array is stored in a large shift register, insertion costs one cycle and

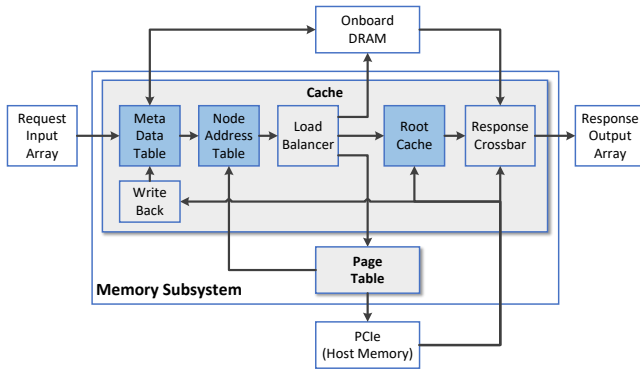


Figure 9: Memory Subsystem

can be overlapped with fetching the next item. Any items with version greater than the operation’s read version are filtered out. After sorting, the RSU uses the indirection array to stream keys to the key comparison pipelines in order.

## 5 Memory subsystem

As shown in Figure 9, the memory subsystem includes the cache and the page table. It caches B-Tree nodes to improve performance by reducing off-chip memory accesses, reducing memory accesses over PCIe, and maximizing the use of available off-chip bandwidth. The root node, which is accessed by all requests, is cached in on-chip memory to save off-chip bandwidth. Other interior nodes are cached in on-board DRAM to reduce PCIe accesses, which both improves request throughput and latency. The load balancer directs some memory accesses over PCIe even when they hit in the cache to use all available off-chip memory bandwidth.

The memory subsystem supports multiple input/output interfaces for parallel access from the interior-node search and leaf-node scan engines. It also maintains a page table mapping node LIDs to node physical addresses. This is exposed over PCIe for write operations to replace subtrees atomically by changing mappings (Section 3.4). When the slow path for a write operation changes a page table mapping, the cache entry for the node with that LID is invalidated. Leaf nodes are not cached to avoid the need for cache invalidations over PCIe for every write operation to the B-Tree.

The metadata table keeps track of cached B-Tree nodes in on-board DRAM. It implements a four-way set associative cache indexed by LIDs. Each entry in a set records the node LID, the physical address, and a 32-bit occupancy map where each bit represents 256 bytes of node data (with 8 KB nodes). The metadata table itself is stored in on-board DRAM. Honeycomb uses a small on-chip metadata cache, which has capacity for 1K entries in the current implementation, to minimize the traffic to on-board DRAM.

On cache misses, the cache module fetches an integral number of 256-byte chunks over PCIe and attempts to write them

back to the cache. The write back module implements a locking scheme to avoid conflicts when the cache is invalidated on page table updates or during B-Tree root updates. The write back operation allocates space for a new node in the cache only if the missing access was to the header and shortcut block of the node. The write back module fills other chunks in the allocated cache space when it reads sorted block segments for the node. When interior nodes cannot fit in the cache, we evict a random node from the same set. We leave more complex cache replacement policies for future investigation.

The metadata table determines if incoming memory read requests are hits or misses, and sends them to the node address table (NAT). The NAT is responsible for ensuring each request has a consistent view of each node it visits. For example, without the NAT, a request could read the shortcut block from the cache and an inconsistent sorted block segment from host memory after the page table entry for the node is updated. The NAT maps the request sequence number to the physical address of the node version first accessed by the request. The NAT entry can be written by both the metadata table and the page table depending on whether the first access by the request to a node is a hit or a miss. When an access to a sorted block hits in the cache, the physical address in the cache entry must match the physical address recorded in the NAT for the request. In case of a mismatch or cache miss, the sorted block segment is always loaded from host memory using the physical address from the NAT for the request.

With large caches, the accelerator can become bottlenecked on accesses to on-board DRAM while underutilizing PCIe bandwidth. To use all available off-chip memory bandwidth, the load balancer directs some memory accesses that hit in the cache to host memory over PCIe. It constantly monitors the number of in-flight operations and the total number of bytes being read by those operations on both DRAM and PCIe interfaces. Then balances load across the two interfaces.

## 6 Evaluation

This section compares Honeycomb with eRPC-Masstree [29, 38], a state-of-the-art ordered key-value store that supports variable-size keys and values (we discuss why we chose this baseline in Section 7). It also evaluates the impact of several optimizations on performance.

### 6.1 Experimental setup

Experiments ran one server on one machine and clients on another. They ran on a single socket of a dual-socket machine because this provided the best cost-performance for both systems. Each socket had a 10-core Intel Xeon E5-2660 v3 @ 2.89 GHz and four channels to 64 GB of DDR4-2133 DRAM. The FPGA accelerator card had an Intel Arria 10 1150 FPGA with two channels to 4 GB on-board DDR4-2133 DRAM, two PCIe Gen3 x8 channels, and 50-Gbps Ethernet. Each



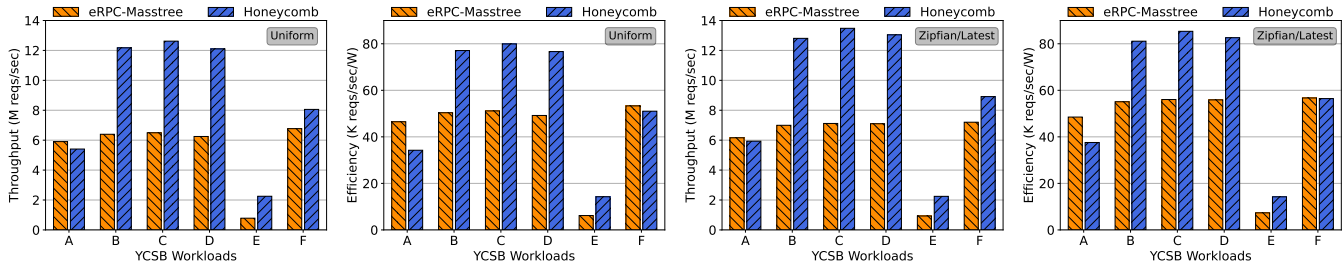


Figure 10: Comparison of throughput and efficiency for YCSB workloads using uniform and Zipfian/latest distributions.

	Logic	Register	Block RAM
Shell	14.0%	8.9%	14.6%
Networking	6.9%	2.4%	21.0%
B-Tree accelerator	33.0%	11.5%	35.6%
Memory subsystem	7.3%	2.9%	7.7%
Total	61.2%	25.7%	78.8%

Table 1: FPGA resource usage of Honeycomb.

	A	B	C	D	E	F
Read Operation	LOOKUP	LOOKUP	LOOKUP	LOOKUP	SCAN (1 to 100)	LOOKUP
Write Operation	UPDATE	UPDATE	-	INSERT	INSERT	RD-MOD-WR
Rd-Wr Ratio (%)	50:50	95:5	100:0	95:5	95:5	50:50 (66.6% LOOKUP)

Table 2: YCSB workloads.

machine had a separate 40-Gbps Ethernet ConnectX-3 NIC. We used the socket that is attached to both the FPGA and the NIC. We ran 10 software threads, each pinned to a different core on the socket. Honeycomb ran on Windows Server 2016 Datacenter using the FPGA, and eRPC-Masintree ran on Ubuntu 20.04 with DPDK 19.11.5 using the ConnectX-3 NIC. Machines were connected to a DELL Z9100-ON switch. The different bandwidths did not affect the comparison because eRPC-Masintree was never bottlenecked on the network.

We configured Honeycomb with MVCC by default even though eRPC-Masintree does not provide linearizability for scans. The modular design of the Honeycomb accelerator enables the user to choose configurations with different numbers of KSUs, RSUs, and MSIs. This is critical to achieving good power efficiency because it allows the user to trade off performance for power and hardware resource efficiency. We used a simple analytic performance model and tuning experiments to select the minimum number of these units to achieve a target SCAN operation throughput of approximately 10 Mops/s. We used 14 KSUs, 4 shortcut-RSUs, 5 log-RSUs, 5 sorted-RSUs, and 4 MSI adapters in all the experiments described in this paper. The accelerator is clocked at 220 MHz. The breakdown of FPGA resource usage is shown in Table 1. The FPGA design tool [26] reports a TDP of 34.9 W.

We ran each experiment three times and present the average

of the results. The range of the results was below 4% of the average for all experiments.

## 6.2 Workloads

We used two sets of workloads in the evaluation YCSB [1, 15] and a *cloud-storage* workload representative of the distributed file system application [9] discussed throughout the paper. We ran all six YCSB workloads (see Table 2) with both uniform and skewed access patterns. The read-modify-write operation in YCSB-F is a combination of a LOOKUP followed by an UPDATE. The cloud-storage workload is similar to YCSB-E but uses shorter scans and we varied the percentage of scans from 50% to 100% to characterize the range of read-write ratios for which Honeycomb is beneficial. We also varied the number of key-value pairs returned by scans and the size of keys and values. In all workloads, insert keys were generated randomly with uniform distribution as in [52]. We used both uniform and Zipfian [15] ( $\theta = 0.99$ ) distributions for lookup keys and the start keys of scans.

All experiments used the uniform distribution, and 16-byte keys and values unless specified otherwise. The store had 128 million key-value pairs in the initial state for all experiments, which are stored in a 4-level tree in Honeycomb. We observed that eRPC-Masintree consumes  $3\times$  more memory than the total size of the key-value pairs to store the whole B-Tree, whereas Honeycomb only consumes about  $1.44\times$ .

## 6.3 Comparison with eRPC-Masintree

Cost-performance is the key metric to optimize in large scale data centers. We use TDP as a proxy for total cost of ownership (TCO) as in [28]. We use a single-socket server for Honeycomb because adding another socket increases TDP without increasing the throughput of the hardware accelerator. We ran experiments with two sockets for eRPC-Masintree but they resulted in worse cost-performance, e.g., it achieved  $1.34\times$  better cost-performance with one socket than with two for read-only 3-item scan workloads. Therefore, we also present single socket results for eRPC-Masintree. We compute TDP by adding numbers for each component from published documentation. The server TDP is 127 W for eRPC-Masintree

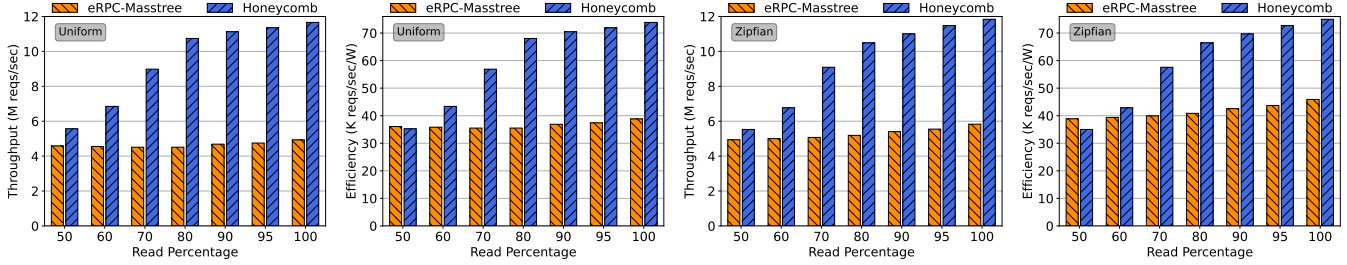


Figure 11: Comparison of throughput and efficiency for cloud-storage workloads with 50% to 100% reads using uniform and Zipfian distributions. The read operation is SCAN with 3 to 4 items in the range.

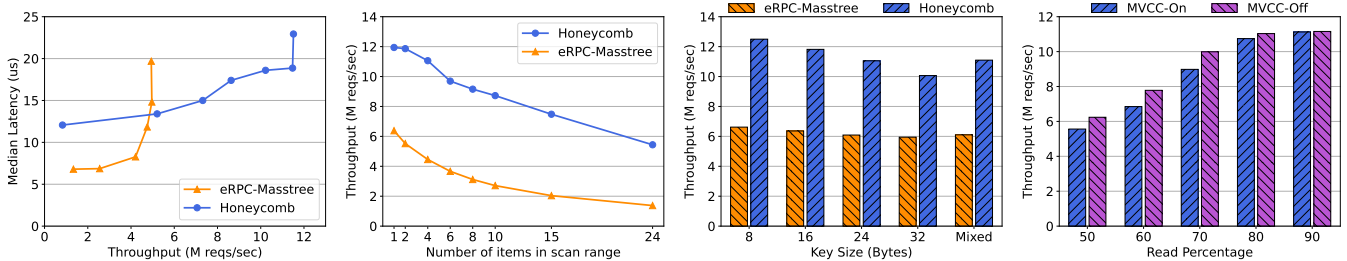


Figure 12: Latency-throughput. Figure 13: Varying SCAN size. Figure 14: Varying key sizes. Figure 15: Impact of MVCC.

and 157.9 W for Honeycomb. The TDP for Honeycomb is larger because it uses a 40-W FPGA accelerator board instead of a 10-W ConnectX-3 NIC [40].

Both the throughput and the TDP should scale by a factor of two when using an additional CPU socket connected to an additional NIC (for eRPC-Masstree) or SmartNIC (for Honeycomb). Therefore, the performance per watt of TDP for such a system would be similar to the results we present with a single socket.

**YCSB throughput and efficiency:** Figure 10 compares both average throughput (Mreqs/s) and throughput per watt of TDP (Kreqs/s/W) of eRPC-Masstree and Honeycomb. Since Honeycomb is not optimized for write-heavy workloads, it is less efficient running YCSB-A and F. For YCSB-B, C and D, Honeycomb improves throughput per watt by  $1.5\times$  with both uniform and Zipfian/latest distributions. It also improves the throughput for these workloads by  $1.9\times$  with uniform and  $1.8\times$  with Zipfian/latest distributions. Since Honeycomb is optimized for scans, it does particularly well in YCSB-E improving throughput by up to  $2.9\times$  and efficiency by up to  $2.3\times$ . Honeycomb is bottlenecked on the network for large scans while eRPC-Masstree is always bottlenecked on the CPU.

**Cloud storage throughput and efficiency:** Figure 11 compares performance and efficiency of eRPC-Masstree and Honeycomb running the cloud-storage workload. In this experiment, the boundary keys in Honeycomb  $SCAN(K_l, K_u)$  requests were chosen to return exactly three items when executed on the initial key-value store. However, they can return between three and four items because of newly-inserted items.

Since eRPC-Masstree provides a different  $SCAN(K, N)$  operation that returns the  $N$  items following  $K$ , we selected a value of  $N$  between three and four to ensure  $SCAN$  operations return the same average number of items in both systems. For high read percentages, Honeycomb also uses CPU cores to execute  $SCAN$  operations. We configured eRPC-Masstree to enable any thread to execute  $SCAN$ s.

The results show that Honeycomb improves both performance and cost-performance significantly for scan-mostly workloads. Since Honeycomb accelerates only read operations, the improvement grows with the read percentage. In the worst case of 100% writes, Honeycomb achieves only 58% of the throughput of eRPC-Masstree (47% of the cost-performance) because there is no hardware acceleration and the B-Tree is optimized for hybrid CPU-FPGA execution. However, even for workloads with 50% writes, Honeycomb achieves a similar throughput per watt as eRPC-Masstree and better throughput ( $1.2\times$  better with uniform distribution). For workloads with at least 80% reads, Honeycomb improves throughput per watt by  $1.9\times$  with uniform and  $1.6\times$  with Zipfian distributions. It also improves the throughput for these workloads by  $2.3\times$  with uniform and  $2.0\times$  with Zipfian distributions.

As in YCSB workloads, the gains from acceleration are lower with the Zipfian distribution. Whereas eRPC-Masstree can leverage better locality with CPU caching, the current implementation of Honeycomb does not cache leaf nodes, which prevents it from caching leaves containing popular items. We plan to explore leaf caching in the future.

With modern cloud storage server designs that leverage

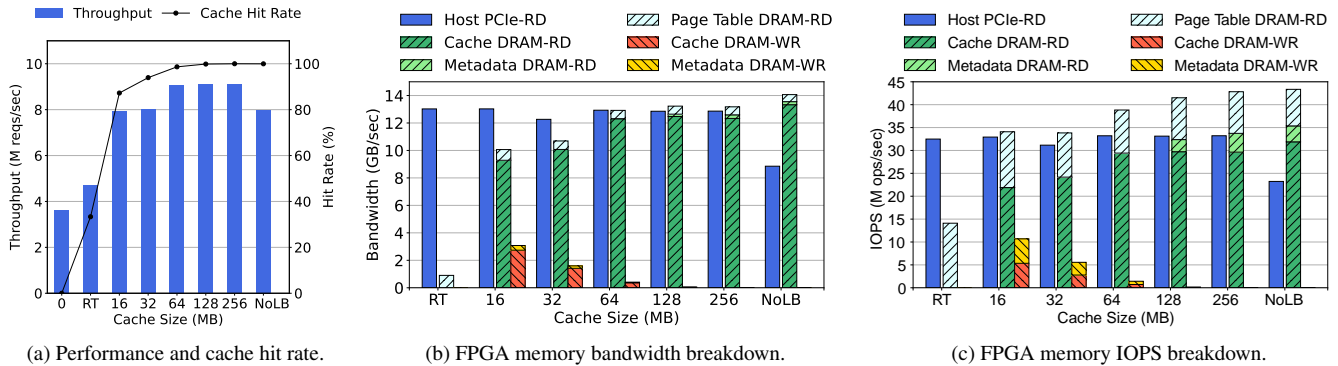


Figure 16: Performance impact of caching and load balancing on Honeycomb (FPGA only) 1-item SCAN.

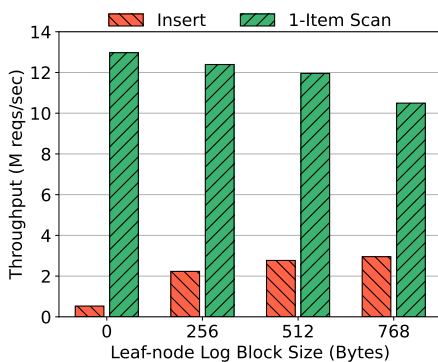


Figure 17: Performance impact of log block size.

NVMe SSDs [44, 49] and fast networks to provide tens of millions of IOPS per server, indexing metadata requires powerful CPUs that account for a large fraction of the overall TCO, e.g., CPUs, DRAM, and the NIC account for half the TDP in Open Compute Project’s Poseidon [31] storage server. Therefore, Honeycomb can significantly increase overall performance per TCO for these storage servers, e.g., we estimate improvements around 20% for server designs similar to Poseidon. This is very significant for large-scale data center deployments.

We expect Honeycomb’s cost-performance gains to increase with future hardware because newer FPGAs have more on-chip memory to cache B-Tree nodes and use PCIe Gen5 that has  $4\times$  the bandwidth of PCIe Gen3. Despite the bandwidth improvement, we expect PCIe to remain the bottleneck because we can use configurations with more KSUs, RSUs, and MSIs to increase parallelism. Therefore, the techniques proposed in this paper will continue to be important.

**End-to-end latency:** Figure 12 shows throughput-latency curves for median latency measured at the client in a read-only workload where each SCAN returns exactly three items. Honeycomb can provide better throughput than eRPC-Masstree’s throughput at lower latency. However, eRPC-Masstree has lower latency at low load. This is mostly because Honeycomb memory accesses over PCIe and to on-board DRAM have

higher latency than CPU memory accesses.

**Scan size:** Figure 13 shows the throughput of both systems for a read-only workload when varying the number of items returned by SCANS. The gains of acceleration increase with scan size, for example, Honeycomb has  $4.0\times$  better throughput and  $3.2\times$  better throughput per watt with 24-item scans. Since eRPC-Masstree must follow pointers to each item in the scan range, these random memory accesses become a bottleneck. Honeycomb can amortize PCIe accesses to a leaf node over many items because it inlines variable-sized items in leaves. With longer scans Honeycomb becomes network bound while eRPC-Masstree remains CPU bound (as observed in YCSB-E).

**Key size:** Figure 14 shows the throughput of both systems running 1-item SCAN on the initial store when the size of keys and values increases (equal key and value sizes). We use 1-item SCAN to better isolate the impact of increasing key sizes on tree traversal. The performance of both systems drops as key size increases. eRPC-Masstree has deeper trees to traverse with larger keys. The depth of the Honeycomb does not change but the accelerator must fetch larger sorted block segments. We also compared both systems on a store with a mix of key and value sizes chosen uniformly from multiples of 8B less than or equal to 32B. These demonstrate that Honeycomb performs well with variable-sized KV pairs.

## 6.4 Impact of optimizations

We ran experiments to investigate the performance impact of using MVCC, log blocks, the cache, and the load balancer.

**Cost of MVCC:** All experiments ran with MVCC to provide linearizable scans. Since eRPC-Masstree does not provide linearizable scans, we also ran experiments to evaluate the impact of MVCC on throughput. Figure 15 shows that turning off MVCC improves Honeycomb performance on cloud-storage workloads by up to 14% when the workload is bottlenecked by INSERTS. The overhead on read-heavy workloads is negligible.

**Log block:** Figure 17 shows throughput of 1-item scans in a read-only workload and of inserts in a write-only workload with varying log block size. Using log blocks improves insert performance because it avoids adding the new item to the sorted block, adjusting shortcuts, and updating the accelerator page table on every operation. However, it reduces SCAN performance because it increases the amount of data accessed over PCIe. Using a 512-byte block achieves most of the benefit while decreasing SCAN throughput by only 8%.

**Accelerator cache and load balancer:** Figure 16 shows the impact of caching on 1-item SCAN throughput in a read-only workload using only the FPGA (no CPU). Figure 16a shows request throughput and cache hit rate for interior node accesses. Caching the root node in on-chip memory (RT) improves performance by 30% over the no-cache case. Adding an on-board DRAM cache with 256 MB (which can hold all interior nodes) improves performance by  $2.5\times$ . The load balancer directs some cache hits to host memory over PCIe to maximize off-chip bandwidth utilization. Removing the load balancer (NoLB) decreases throughput by 13%.

Figures 16b and 16c break down bandwidth and IOPS for PCIe and on-board DRAM traffic. For small cache sizes, the bottleneck is PCIe bandwidth and there are writes to on-board DRAM due to cache replacement. With a 256 MB cache (100% hit rate) and no load balancing (NoLB), on-board DRAM bandwidth is the bottleneck while 4 GB/s of PCIe bandwidth is left unused. The load balancer shifts traffic to PCIe to maximize off-chip bandwidth utilization increasing throughput from 8.0 to 9.1 Mreqs/s. Page table and cache metadata reads consume a small fraction of available on-board DRAM bandwidth but a significant fraction of IOPS. For small cache sizes, there are no metadata reads from on-board DRAM because all metadata fits in the on-chip cache.

## 7 Related work

We build on a large body of work on indices for in-memory ordered key-value stores (e.g., [33,34,38,51,54]). A comparison study [51] showed that the Adaptive Radix Tree (ART) [33] performed best followed by Masstree [38] except on scan-dominated workloads where a B+ tree [13] variant was better. We chose Masstree [38] as a baseline because it has better scan performance than ART and it supports variable-size keys unlike the B+ tree variant in [51]. Cuckoo Trie [54] exploits memory level parallelism to improve multi-core performance but it has worse scan performance than ART. None of these indices supports linearizable scans. Given our focus on scan-dominated workloads, Honeycomb implements a B+ tree variant with support for variable-size keys and MVCC. Many of the optimizations in recent work exploit the memory hierarchy of modern server-class CPUs and are not applicable to Honeycomb where the index is accessed over PCIe.

Ordered key-value stores shard an index across servers and provide access to remote clients across the network. Re-

cent research has shown how to leverage kernel-bypass using DPDK [27] to implement eRPC [29], a fast RPC mechanism. eRPC and Masstree have been used to implement a high throughput, low-latency, key-value store [29] that we use as our baseline. Other research has explored using one-sided RDMA reads to bypass the server CPU for GET and SCAN operations [12, 18, 41, 52, 56]. Since RDMA NICs only provide simple reads of contiguous memory, these systems require at least two RDMA reads per operation to support variable-sized keys or values, and they use client-side caching to avoid additional RDMA reads when traversing the index. XStore [52] uses a learned cache, a compact client-side cache design inspired by the work on learned indices [16, 32], but it does not support variable-sized keys or linearizable SCANS.

CliqueMap [48] implements a hybrid in-memory key-value caching system with both RPC and remote memory access (RMA). Like Honeycomb, it accelerates GET with RMA and executes SET via RPC to save CPU cost and improve performance. However, this implementation is based on a hash table and does not provide support for efficient SCANS.

There are proposals to extend RDMA, e.g., [2, 8], but these have yet to be implemented in NIC hardware.

SmartNICs avoid the functionality limitations of RDMA by providing programmable processing engines in the NIC. There are two types: SoC-based with general purpose cores and accelerators for common functionality like compression and encryption (see [37] for a survey); and FPGA-based [10, 45]. Since the later offer the promise of better performance and energy efficiency at the cost of being harder to program, Honeycomb leverages an FPGA-based SmartNIC but implements complex split and merge of B-Tree nodes on the host CPU.

SmartNICs have been used as offloads for accelerating networking, e.g., [3, 6, 19–21, 36, 43], AI inference [22], distributed file systems [30], transactions [47], unordered key-value stores [11, 19, 35, 46], and ordered key-value stores [23, 37, 53].

KV-direct [35], which is the best unordered key-value store offload, stores the index in host memory and implements hash table reads and writes, which are much simpler than B-Tree writes, in the FPGA. It achieves better performance than Honeycomb because this reduces synchronization across PCIe and hash table operations only require  $O(1)$  memory accesses, but it does not provide SCANS. The best ordered key-value store offload, HeteroKV [53], implements a B-Tree where the leaves are hash tables, which results in poor scan performance. It cannot support large stores because it stores the B-Tree in on-chip FPGA memory, and it supports only fixed-size keys. Honeycomb provides support for large stores, variable-sized keys and values, fast scans, and strong consistency.

## 8 Conclusion

In-memory ordered key-value stores are an important building block in modern distributed applications. We presented Honeycomb, a system that leverages an FPGA-based SmartNIC to accelerate these stores with a focus on scan-dominated workloads. It stores a B-Tree in host memory, and executes SCAN and GET operations on the FPGA, and PUT, UPDATE, and DELETE operations on the CPU. This approach enables large stores and simplifies the FPGA implementation but raises the challenge of data access and synchronization across slow PCIe. We described how Honeycomb addresses this challenge by using large B-Tree nodes with shortcuts; caching in on-chip and on-board FPGA memory; exploiting request-level parallelism with out-of-order execution; making SCAN and GET operations wait free; and using a log in B-Tree nodes to batch synchronization across PCIe. Honeycomb is evaluated against a state-of-the-art ordered key-value store using both YCSB and a cloud-storage-inspired workload. The comparison shows that Honeycomb improves throughput by  $1.9\times$  for uniform read-dominated workloads in YCSB and by  $2.3\times$  for uniform cloud-storage-inspired workloads with more than 80% SCAN operations. Most importantly, Honeycomb improves cost-performance, which is the key metric to optimize in large-scale data centers; it improves throughput per watt of TDP (a proxy for TCO) by more than  $1.5\times$  and  $1.9\times$  for these two set of workloads respectively.

## Acknowledgments

We thank Vadim Makhervaks, Lukasz Tomczyk, Prahasaran Asokan, and Ankit Agrawal for their help and discussions on exploring Honeycomb in cloud storage services. We thank Andrew Putnam for his support and help with onboarding Catapult FPGA platform. We thank Nikita Lazarev, David Sidler, Mikhail Asiatici and Fabio Maschi who worked on related projects during their internships at Microsoft Research. We thank the members of Cloud System Futures team in Microsoft Research Cambridge for their help and feedback.

## References

- [1] Github repository of YCSB. <https://github.com/brianfrankcooper/YCSB>.
- [2] Marcos K Aguilera, Kimberly Keeton, Stanko Novakovic, and Sharad Singhal. Designing far memory data structures: Think outside the box. In *Proceedings of the Workshop on Hot Topics in Operating Systems*, pages 120–126, 2019.
- [3] Mina Tahmasbi Arashloo, Alexey Lavrov, Manya Ghobadi, Jennifer Rexford, David Walker, and David Wentzlaff. Enabling programmable transport protocols in high-speed nics. In *17th USENIX Symposium on Networked Systems Design and Implementation (NSDI 20)*, pages 93–109, 2020.
- [4] Berk Atikoglu, Yuehai Xu, Eitan Frachtenberg, Song Jiang, and Mike Paleczny. Workload analysis of a large-scale key-value store. In *Proceedings of the 12th ACM SIGMETRICS/PERFORMANCE joint international conference on Measurement and Modeling of Computer Systems*, pages 53–64, 2012.
- [5] Philip A Bernstein, Vassos Hadzilacos, and Nathan Goodman. *Concurrency control and recovery in database systems*, volume 370. Addison-wesley Reading, 1987.
- [6] Marco Spaziani Brunella, Giacomo Belocchi, Marco Bonola, Salvatore Pontarelli, Giuseppe Siracusano, Giuseppe Bianchi, Aniello Cammarano, Alessandro Palumbo, Luca Petrucci, and Roberto Bifulco. hxdp: Efficient software packet processing on {FPGA} nics. In *14th {USENIX} Symposium on Operating Systems Design and Implementation ({OSDI} 20)*, pages 973–990, 2020.
- [7] Chiranjeev Buragohain, Knut Magne Risvik, Paul Brett, Miguel Castro, Wonhee Cho, Joshua Cowhig, Nikolas Gloy, Karthik Kalyanaraman, Richendra Khanna, John Pao, et al. A1: A distributed in-memory graph database. In *Proceedings of the 2020 ACM SIGMOD International Conference on Management of Data*, pages 329–344, 2020.
- [8] Matthew Burke, Shannon Joyner, Adriana Szekeres, Jacob Nelson, Irene Zhang, and Dan RK Ports. Prism: Rethinking the rdma interface for distributed systems. In *Proceedings of the ACM SIGOPS 28th Symposium on Operating Systems Principles CD-ROM*, pages 228–242, 2021.
- [9] Brad Calder, Ju Wang, Aaron Ogus, Niranjana Nilakantan, Arild Skjolsvold, Sam McKelvie, Yikang Xu, Shashwat Srivastav, Jiesheng Wu, Huseyin Simitci, et al. Windows azure storage: a highly available cloud storage service with strong consistency. In *Proceedings of the Twenty-Third ACM Symposium on Operating Systems Principles*, pages 143–157, 2011.
- [10] Adrian M. Caulfield, Eric S. Chung, Andrew Putnam, Hari Angepat, Jeremy Fowers, Michael Haselman, Stephen Heil, Matt Humphrey, Puneet Kaur, Joo-Young Kim, Daniel Lo, Todd Massengill, Kalin Ovtcharov, Michael Papamichael, Lisa Woods, Sitaram Lanka, Derek Chiou, and Doug Burger. A cloud-scale acceleration architecture. In *The 49th Annual IEEE/ACM International Symposium on Microarchitecture, MICRO-49*, Taipei, Taiwan, 2016. IEEE Press.

- [11] Sai Rahul Chalamalasetti, Kevin Lim, Mitch Wright, Alvin AuYoung, Parthasarathy Ranganathan, and Martin Margala. An fpga memcached appliance. In *Proceedings of the ACM/SIGDA international symposium on Field programmable gate arrays*, pages 245–254, 2013.
- [12] Yanzhe Chen, Xingda Wei, Jiashin Shi, Rong Chen, and Haibo Chen. Fast and general distributed transactions using rdma and htm. In *Proceedings of the Eleventh European Conference on Computer Systems*, pages 1–17, 2016.
- [13] Douglas Comer. Ubiquitous b-tree. *ACM Computing Surveys (CSUR)*, 11(2):121–137, 1979.
- [14] Redis community. redis. <https://redis.io/>.
- [15] Brian F Cooper, Adam Silberstein, Erwin Tam, Raghu Ramakrishnan, and Russell Sears. Benchmarking cloud serving systems with ycsb. In *Proceedings of the 1st ACM symposium on Cloud computing*, pages 143–154, 2010.
- [16] Jialin Ding, Umar Farooq Minhas, Jia Yu, Chi Wang, Jaeyoung Do, Yinan Li, Hantian Zhang, Badrish Chandramouli, Johannes Gehrke, Donald Kossmann, et al. Alex: an updatable adaptive learned index. In *Proceedings of the 2020 ACM SIGMOD International Conference on Management of Data*, pages 969–984, 2020.
- [17] Siying Dong, Mark Callaghan, Leonidas Galanis, Dhruva Borthakur, Tony Savor, and Michael Strum. Optimizing space amplification in rocksdb. In *CIDR*, volume 3, page 3, 2017.
- [18] Aleksandar Dragojević, Dushyanth Narayanan, Edmund B Nightingale, Matthew Renzelmann, Alex Shamis, Anirudh Badam, and Miguel Castro. No compromises: Distributed transactions with consistency, availability, and performance. In *Proceedings of the 25th symposium on operating systems principles*, pages 54–70, 2015.
- [19] Haggai Eran, Lior Zeno, Maroun Tork, Gabi Malka, and Mark Silberstein. {NICA}: An infrastructure for inline acceleration of network applications. In *2019 USENIX Annual Technical Conference (USENIX ATC 19)*, pages 345–362, 2019.
- [20] Daniel Firestone. {VFP}: A virtual switch platform for host {SDN} in the public cloud. In *14th {USENIX} Symposium on Networked Systems Design and Implementation ({NSDI} 17)*, pages 315–328, 2017.
- [21] Daniel Firestone, Andrew Putnam, Hari Angepat, Derek Chiou, Adrian Caulfield, Eric Chung, Matt Humphrey, Kalin Ovtcharov, Jitu Padhye, Doug Burger, Dave Maltz, Albert Greenberg, Sambhrama Mundkur, Alireza Dabagh, Mike Andrewartha, Vivek Bhanu, Harish Kumar Chandrappa, Somesh Chaturmohta, Jack Lavier, Norman Lam, Fengfen Liu, Gautham Popuri, Shachar Raindel, Tejas Sapre, Mark Shaw, Gabriel Silva, Madhan Sivakumar, Nisheeth Srivastava, Anshuman Verma, Qasim Zuhair, Deepak Bansal, Kushagra Vaid, and David A. Maltz. Azure accelerated networking: Smart-nics in the public cloud. In *15th USENIX Symposium on Networked Systems Design and Implementation (NSDI)*, April 2018.
- [22] Jeremy Fowers, Kalin Ovtcharov, Michael Papamichael, Todd Massengill, Ming Liu, Daniel Lo, Shlomi Alkalay, Michael Haselman, Logan Adams, Mahdi Ghandi, Stephen Heil, Prerak Patel, Adam Sapek, Gabriel Weisz, Lisa Woods, Sitaram Lanka, Steve Reinhardt, Adrian Caulfield, Eric Chung, and Doug Burger. A configurable cloud-scale dnn processor for real-time ai. In *Proceedings of the 45th International Symposium on Computer Architecture, 2018*. ACM, June 2018.
- [23] Dennis Heinrich, Stefan Werner, Marc Stelzner, Christopher Blochwitz, Thilo Pionteck, and Sven Groppe. Hybrid fpga approach for a b+ tree in a semantic web database system. In *2015 10th International Symposium on Reconfigurable Communication-centric Systems-on-Chip (ReCoSoC)*, pages 1–8. IEEE, 2015.
- [24] Maurice Herlihy. Wait-free synchronization. *ACM Transactions on Programming Languages and Systems (TOPLAS)*, 13(1):124–149, 1991.
- [25] Maurice P Herlihy and Jeannette M Wing. Linearizability: A correctness condition for concurrent objects. *ACM Transactions on Programming Languages and Systems (TOPLAS)*, 12(3):463–492, 1990.
- [26] Intel. Intel Quartus Prime Pro Edition User Guide: Power Analysis and Optimization. <https://www.intel.com/content/www/us/en/programmable/documentation/osq1513989409475.html>, 2021.
- [27] DPK Intel. Data plane development kit, 2014.
- [28] Norman P Jouppi, Doe Hyun Yoon, Matthew Ashcraft, Mark Gottscho, Thomas B Jablin, George Kurian, James Laudon, Sheng Li, Peter Ma, Xiaoyu Ma, et al. Ten lessons from three generations shaped google’s tpuv4i: Industrial product. In *2021 ACM/IEEE 48th Annual International Symposium on Computer Architecture (ISCA)*, pages 1–14. IEEE, 2021.
- [29] Anuj Kalia, Michael Kaminsky, and David Andersen. Datacenter rpcs can be general and fast. In *16th {USENIX} Symposium on Networked Systems Design and Implementation ({NSDI} 19)*, pages 1–16, 2019.

- [30] Jongyul Kim, Insu Jang, Waleed Reda, Jaeseong Im, Marco Canini, Dejan Kostić, Youngjin Kwon, Simon Peter, and Emmett Witchel. Linefs. In *Proceedings of the ACM SIGOPS 28th Symposium on Operating Systems Principles CD-ROM*. ACM, 2021.
- [31] Jungsoo Kim and Alan Chang. Poseidon V1 E1.S SSD Storage System. <https://www.opencompute.org/documents/poseidon-v1-reference-system-spec-pdf>, 2022.
- [32] Tim Kraska, Alex Beutel, Ed H Chi, Jeffrey Dean, and Neoklis Polyzotis. The case for learned index structures. In *Proceedings of the 2018 International Conference on Management of Data*, pages 489–504, 2018.
- [33] Viktor Leis, Alfons Kemper, and Thomas Neumann. The adaptive radix tree: Artful indexing for main-memory databases. In *2013 IEEE 29th International Conference on Data Engineering (ICDE)*, pages 38–49. IEEE, 2013.
- [34] Justin J. Levandoski, David B. Lomet, and Sudipta Sen-gupta. The bw-tree: A b-tree for new hardware platforms. In *2013 IEEE 29th International Conference on Data Engineering (ICDE)*, pages 302–313, 2013.
- [35] Bojie Li, Zhenyuan Ruan, Wencong Xiao, Yuanwei Lu, Yongqiang Xiong, Andrew Putnam, Enhong Chen, and Lintao Zhang. Kv-direct: High-performance in-memory key-value store with programmable nic. In *Proceedings of the 26th Symposium on Operating Systems Principles*, pages 137–152, 2017.
- [36] Bojie Li, Kun Tan, Layong Luo, Yanqing Peng, Ren-qian Luo, Ningyi Xu, Yongqiang Xiong, Peng Cheng, and Enhong Chen. Clicknp: Highly flexible and high performance network processing with reconfigurable hardware. In *Proceedings of the 2016 ACM SIGCOMM Conference*, pages 1–14, 2016.
- [37] Ming Liu, Tianyi Cui, Henry Schuh, Arvind Krishnamurthy, Simon Peter, and Karan Gupta. Offloading distributed applications onto smartnics using ipipe. In *Proceedings of the ACM Special Interest Group on Data Communication*, pages 318–333. 2019.
- [38] Yandong Mao, Eddie Kohler, and Robert Tappan Morris. Cache craftiness for fast multicore key-value storage. In *Proceedings of the 7th ACM european conference on Computer Systems*, pages 183–196, 2012.
- [39] Paul E McKenney and Jonathan Walpole. What is rcu, fundamentally? *Linux Weekly News (LWN.net)*, 2007.
- [40] Mellanox. ConnectX-3 VPI Single and Dual QSFP Port Adapter Card User Manual. [https://www.mellanox.com/related-docs/user-manuals/ConnectX-3\\_VPI\\_Single\\_and\\_Dual\\_QSFP\\_Port\\_Adapter\\_Card\\_User\\_Manual.pdf](https://www.mellanox.com/related-docs/user-manuals/ConnectX-3_VPI_Single_and_Dual_QSFP_Port_Adapter_Card_User_Manual.pdf), 2013.
- [41] Christopher Mitchell, Kate Montgomery, Lamont Nelson, Siddhartha Sen, and Jinyang Li. Balancing {CPU} and network in the cell distributed b-tree store. In *2016 {USENIX} Annual Technical Conference ({USENIX}{ATC} 16)*, pages 451–464, 2016.
- [42] Rajesh Nishtala, Hans Fugal, Steven Grimm, Marc Kwiatkowski, Herman Lee, Harry C Li, Ryan McElroy, Mike Paleczny, Daniel Peek, Paul Saab, et al. Scaling memcache at facebook. In *10th {USENIX} Symposium on Networked Systems Design and Implementation ({NSDI} 13)*, pages 385–398, 2013.
- [43] Phitchaya Mangpo Phothilimthana, Ming Liu, Antoine Kaufmann, Simon Peter, Rastislav Bodik, and Thomas Anderson. Floem: A programming system for nic-accelerated network applications. In *13th {USENIX} Symposium on Operating Systems Design and Implementation ({OSDI} 18)*, pages 663–679, 2018.
- [44] Open Compute Project. Samsung PM9A3 NVMe PCIe SSD. <https://www.opencompute.org/products/262/samsung-pm9a3-nvme-pcie-ssd>.
- [45] Andrew Putnam, Adrian M. Caulfield, Eric S. Chung, Derek Chiou, Kypros Constantinides, John Demme, Hadi Esmaeilzadeh, Jeremy Fowers, Gopi Prashanth Gopal, Jan Gray, Michael Haselman, Scott Hauck, Stephen Heil, Amir Hormati, Joo-Young Kim, Sitaram Lanka, James Larus, Eric Peterson, Simon Pope, Aaron Smith, Jason Thong, Phillip Yi Xiao, and Doug Burger. A reconfigurable fabric for accelerating large-scale data-center services. In *Proceeding of the 41st Annual International Symposium on Computer Architecture, ISCA '14*, page 13–24, Minneapolis, Minnesota, USA, 2014. IEEE Press.
- [46] Yuchen Ren, Jinyu Xie, Yunhui Qiu, Hankun Lv, Wenbo Yin, Lingli Wang, Bowei Yu, Hua Chen, Xianjun He, Zhijian Liao, et al. A low-latency multi-version key-value store using b-tree on an fpga-cpu platform. In *2019 29th International Conference on Field Programmable Logic and Applications (FPL)*, pages 321–325. IEEE, 2019.
- [47] Henry N Schuh, Weihao Liang, Ming Liu, Jacob Nelson, and Arvind Krishnamurthy. Xenix: Smartnic-accelerated distributed transactions. In *Proceedings of the ACM SIGOPS 28th Symposium on Operating Systems Principles*, pages 740–755, 2021.
- [48] Arjun Singhvi, Aditya Akella, Maggie Anderson, Rob Cauble, Harshad Deshmukh, Dan Gibson, Milo M. K. Martin, Amanda Strominger, Thomas F. Wenisch, and

- Amin Vahdat. Cliquemap: Productionizing an rma-based distributed caching system. In *Proceedings of the 2021 ACM SIGCOMM 2021 Conference, SIGCOMM '21*, page 93–105, New York, NY, USA, 2021. Association for Computing Machinery.
- [49] Ross Stenfort, Ta-Yu Wu, Lee Prewitt, Paul Kaler, David Derosa, William Lynn, and Austin Bolen. Datacenter NVMe SSD Specification. <https://www.opencompute.org/documents/datacenter-nvme-ssd-specification-v2-0r21-pdf>, 2021.
- [50] Venkateshwaran Venkataramani, Zach Amsden, Nathan Bronson, George Cabrera III, Prasad Chakka, Peter Dimov, Hui Ding, Jack Ferris, Anthony Giardullo, Jeremy Hoon, et al. Tao: how facebook serves the social graph. In *Proceedings of the 2012 ACM SIGMOD International Conference on Management of Data*, pages 791–792, 2012.
- [51] Ziqi Wang, Andrew Pavlo, Hyeontaek Lim, Viktor Leis, Huanchen Zhang, Michael Kaminsky, and David G Andersen. Building a bw-tree takes more than just buzz words. In *Proceedings of the 2018 International Conference on Management of Data*, pages 473–488, 2018.
- [52] Xingda Wei, Rong Chen, and Haibo Chen. Fast rdma-based ordered key-value store using remote learned cache. In *14th {USENIX} Symposium on Operating Systems Design and Implementation ({OSDI} 20)*, pages 117–135, 2020.
- [53] Haichang Yang, Zhaoshi Li, Jiawei Wang, Shouyi Yin, Shaojun Wei, and Leibo Liu. Heterokv: A scalable line-rate key-value store on heterogeneous cpu-fpga platforms. In *2021 Design, Automation & Test in Europe Conference & Exhibition (DATE)*, pages 834–837. IEEE, 2021.
- [54] Adar Zeitak and Adam Morrison. Cuckoo trie: Exploiting memory-level parallelism for efficient dram indexing. In *Proceedings of the ACM SIGOPS 28th Symposium on Operating Systems Principles*, pages 147–162, 2021.
- [55] Yibo Zhu, Haggai Eran, Daniel Firestone, Chuanxiong Guo, Marina Lipshteyn, Yehonatan Liron, Jitendra Padhye, Shachar Raindel, Mohamad Haj Yahia, and Ming Zhang. Congestion control for large-scale rdma deployments. *ACM SIGCOMM Computer Communication Review*, 45(4):523–536, 2015.
- [56] Tobias Ziegler, Sumukha Tumkur Vani, Carsten Binnig, Rodrigo Fonseca, and Tim Kraska. Designing distributed tree-based index structures for fast rdma-capable networks. In *Proceedings of the 2019 International Conference on Management of Data*, pages 741–758, 2019.